BIOPHYSICS

The nonconducting W434F mutant adopts upon membrane depolarization an inactivated-like state that differs from wild-type Shaker-IR potassium channels

Laura Coonen[1], Evelyn Martinez-Morales[1], Dieter V. Van De Sande[1], Dirk J. Snyders[1], D. Marien Cortes[2], Luis G. Cuello[2]*, Alain J. Labro[1,3]*

Voltage-gated K^+ (Kv) channels mediate the flow of K^+ across the cell membrane by regulating the conductive state of their activation gate (AG). Several Kv channels display slow C-type inactivation, a process whereby their selectivity filter (SF) becomes less or nonconductive. It has been proposed that, in the fast inactivation-removed Shaker-IR channel, the W434F mutation epitomizes the C-type inactivated state because it functionally accelerates this process. By introducing another pore mutation that prevents AG closure, P475D, we found a way to record ionic currents of the Shaker-IR-W434F-P475D mutant at hyperpolarized membrane potentials as the W434F-mutant SF recovers from its inactivated state. This W434F conductive state lost its high K^+ over Na^+ selectivity, and even $NMDG^+$ can permeate, features not observed in a wild-type SF. This indicates that, at least during recovery from inactivation, the W434F-mutant SF transitions to a widened and noncationic specific conformation.

INTRODUCTION

Voltage-gated potassium K^+ channels (Kv channels) form transmembrane K^+ permeation pathways that are regulated by changes in the cell membrane potential (*1*). The molecular basis of the gating mechanisms underlying these voltage-dependent changes in ion conductivity have been extensively studied in the Shaker and Shaker-type Kv channels (*2*). The Shaker channel has the typical Kv channel membrane topology existing in the cell membrane as a tetramer of α subunits, each consisting of six membrane-spanning helices (S1 to S6) (*3*, *4*). The S5 and S6 segments assemble into the K^+ permeation pathway with a voltage-controlled activation gate (AG) at the intracellular bundle crossing point of the S6 segments (*5*, *6*). The channel's voltage-sensing domains (VSDs), which are composed of the S1 to S4 segments, detect changes in the cell membrane potential that triggers a conformational change in the VSDs, which is translated into the opening or closure of the AG (also known as electromechanical coupling) (*7*–*9*). The bottom parts of the S6 segments have at the vicinity of the bundle crossing point, a double proline (PVP) motif that is conserved in the Shaker-type Kv channels. It has been hypothesized that these prolines introduce flexibility in the S6 by destabilizing its α-helical structure (*10*–*12*), hence forming a hinge point that allows the conformational changes associated with AG opening and closure (*6*, *13*, *14*).

The selectivity filter (SF) within the channel's K^+ selective pore domain is formed by a stretch of amino acid residues between the S5 and S6 segments known as the pore loop (the P-loop), which is located at the extracellular side of the K^+ permeation pathway (*1*, *4*). Besides dictating ion selectivity, the SF serves as an additional gate that can abolish ion conduction by a process termed slow or C-type inactivation (*7*, *15*). C-type inactivation is a rearrangement of the SF that occurs upon prolonged membrane depolarization, triggered by the opening of the AG (*16*–*20*). During hyperpolarization, as the AG closes, channels recover from their C-type inactivated state, i.e., the SF readopts its conductive conformation (*21*, *22*). Thus, at resting negative cell membrane potentials, the Shaker channels have their AG closed and presumably their SF in the conductive state (*23*, *24*). Then, upon membrane depolarization, the VSDs reorient and initiate a sequence of conformational changes that, after passing several intermediate closed states, lead to the opening of the AG (*7*–*9*). When depolarization is sustained, the channels slowly enter the C-type inactivated state, which results in a gradual decrease of the K^+ current (*15*). Initiation of C-type inactivation has been reported to involve different regions of a K^+ channel that are allosterically coupled: a coupling between the AG and the SF (*25*–*32*) and/or a direct communication between the VSD and the SF (*33*).

In a wild-type (WT) Shaker channel, the dimensions of the outer pore region and the four K^+ binding sites within the SF are well maintained by several aromatic amino acids that create a so-called aromatic cuff (*4*, *5*, *34*). The W434 is one of these aromatic amino acids and interacts with Y445 of the TTVGYG K^+ selective signature sequence, thereby contributing to the coordination of K^+ (*35*, *36*). Substituting W434 in the fast inactivation-removed Shaker channel (Shaker-IR) by a phenylalanine (W434F) accelerates and deepens substantially the C-type inactivation process such that the SF becomes nonconductive immediately upon AG opening, ceasing ion conduction (*22*, *37*). In K^+-free conditions, Na^+-currents could be recorded from the Shaker-IR-W434F channel, similar to WT Shaker-IR channels that are C-type inactivated (*38*, *39*). This strengthened the hypothesis that, in a K^+-free condition, the Shaker channel's SF C-type inactivated state adopts a conformation similar to the W434F mutation, which are not physiologically relevant conformations. Here, we investigated the conductance of the W434F mutant channel when it recovers from inactivation at hyperpolarized membrane potentials in physiologically relevant ionic conditions (*22*). Whereas hyperpolarization relieves C-type inactivation, it also promotes AG closure, which represented a methodological challenge as both the SF and

[1]Department of Biomedical Sciences, Faculty of Pharmaceutical, Biomedical and Veterinary Sciences, University of Antwerp, 2610 Antwerp, Belgium. [2]Cell Physiology and Molecular Biophysics, Center for Membrane Protein Research, Texas Tech University Health Sciences Center, Lubbock, TX 79430, USA. [3]Department of Basic and Applied Medical Sciences, Faculty of Medicine, Ghent University, 9000 Ghent, Belgium.
*Corresponding author. Email: luis.cuello@ttuhsc.edu (L.G.C.); alain.labro@ugent.be (A.J.L)

the AG need to be conductive to record ion channel currents. It has been reported that hydrophilic mutations at the second proline of the PVP motif (P475) destabilize the closed conformation of the AG, facilitating ion conduction in the otherwise closed state (*40*, *41*). Addition of the P475D mutation in Shaker-IR-W434F yielded channels that were conductive at hyperpolarizing potentials when the AG closes and the W434F-mutant SF recovers from inactivation. The recorded current was not cation selective, indicating that the Shaker-IR-W434F-P475D SF adopted a conformation that is not K^+ over Na^+ selective. This was not observed in Shaker-IR-P475D channels, suggesting that the inactivated conformation of the W434F-mutant SF does not reflect on the naturally occurring C-type inactivated state of the Shaker-IR WT SF.

RESULTS

Shaker-IR-P475D mutant channels produce large, inward currents during hyperpolarization

The P475D mutant in the Shaker-IR channel (the second proline of the PVP motif was substituted for an aspartate) has been previously characterized in *Xenopus* oocytes as an expression system, but in this work, we have characterized this mutant (Shaker-IR-P475D) expressed in human embryonic kidney (HEK) 293 cells. In accordance with previous reports, HEK293 cells expressing the Shaker-IR-P475D should display both a voltage-dependent and a constitutive K^+ current component as the AG does not close completely (*40*, *41*). Applying depolarizing voltage steps after a 5-s prepulse of −100 mV elicited voltage-dependent current activations (Fig. 1A). The analysis of the instantaneous current amplitude at the different voltage steps indicated the presence of a constitutive K^+ selective current, which originated from an incompletely closed AG (Fig. 1B). Compared to *Xenopus* oocytes, human HEK293 cells do not tolerate well long-lasting negative membrane potentials. This technical limitation precluded the use of very negative holding potentials (i.e., −110 mV), as it was used in the original characterization of the Shaker-IR-P475D mutant (*40*). When voltage steps more negative than −100 mV were applied, a time-dependent increase in current amplitude was observed (Fig. 1A). We reasoned that Shaker-IR-P475D channels most likely should undergo C-type inactivation; therefore, this current increase at negative membrane potentials should originate from channels recovering from C-type inactivation (fig. S1). To characterize the voltage dependency of this time-dependent current at negative membrane potentials, from a holding potential of −70 mV, voltage steps ranging from −140 to +60 mV were applied followed by a voltage step to −20 mV to elicit tail currents (Fig. 2A). Analyzing these tail currents yielded the current-voltage relation (*I-V* curve) that reported on the voltage dependency of Shaker-IR-P475D channels recovering from their inactivated state (Fig. 2B).

Introducing the W434F mutation in Shaker-IR yielded nonconducting channels (fig. S2) (*42*). It is generally accepted that Shaker-IR-W434F's nonconductivity originates from ultrafast channel inactivation. To study the recovery of this mutant from its nonconductive inactivated-like state, we aimed to record ionic currents during hyperpolarization, when the AG closes and drives the SF to recover from its inactivated state (*22*). Here, the P475D mutation was introduced, and the resulting Shaker-IR-W434F-P475D mutant channel displayed large, voltage- and time-dependent inward currents upon membrane hyperpolarization (Fig. 2A). At depolarizing membrane potentials, on the other hand, these channels did not display currents when using an interpulse holding level of −70 mV. Most likely, this happens because the channels are completely inactivated at this holding potential. To validate this assumption and to exclude the possibility that the absence of outward current originates from intracellular Mg^{2+} block, as the P475D mutation introduces an intracellular Mg^{2+} binding site (*43*), similar experiments were performed in solutions without divalent cations. Using intracellular solutions (ICS) without Mg^{2+}, the current recordings of Shaker-IR-W434F-P475D were comparable, yielding large inward currents at hyperpolarized membrane potentials with the absence of current activation at depolarizing potentials (fig. S3). Thus, the time- and voltage-dependent currents of Shaker-IR-W434F-P475D at hyperpolarizing negative membrane potentials likely originated from channels recovering from their inactivated state, as was the case for Shaker-IR-P475D channels. Generating the *I-V* curve for Shaker-IR-W434F-P475D displayed a V_{mid} of −113.7 ± 0.4 mV (N = 9), compared to a V_{mid} of −99.1 ± 3.9 mV (N = 5) for Shaker-IR-P475D (Fig. 2B). Fitting the current increase at hyperpolarization resulted in similar time constants for both Shaker-IR-P475D and Shaker-IR-W434F-P475D (Fig. 2C). Noticeably, during prolonged hyperpolarization, the current amplitude decreased slightly in both P475D

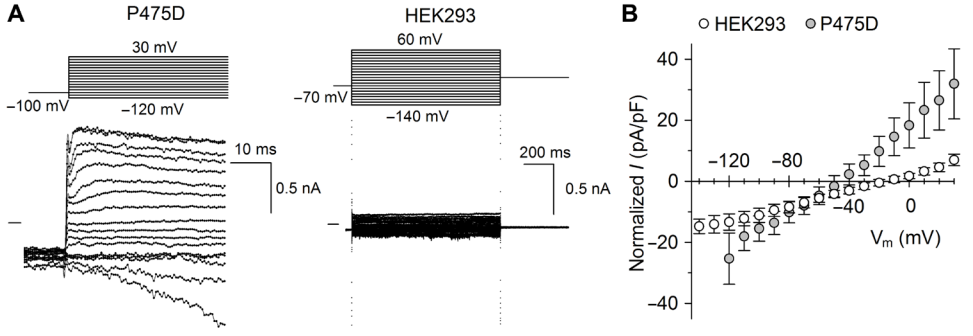

Fig. 1. Shaker-IR-P475D is constitutively conductive. (**A**) Representative whole-cell current recordings from Shaker-IR-P475D expressed in HEK293 cells (left) and HEK293 cells transfected only with the peGFP-n1 marker (right) using the pulse protocols shown on top. For Shaker-IR-P475D, a 5-s prepulse of −100 mV was applied, thereby revealing outward currents upon subsequent depolarization. Interpulse time was 15 s, with a holding potential of −70 mV for both experiments. The horizontal bar at the start of the current traces indicates the zero-current level. (**B**) Current-voltage curve of the instantaneous currents in the Shaker-IR-P475D–expressing HEK293 cells and the peGFP-n1–transfected HEK293 cells. V_{rev} is around −50 mV for Shaker-IR-P475D (gray circles; N = 5) and around 0 mV for the peGFP-n1–transfected HEK293 cells (white circles; N = 3).

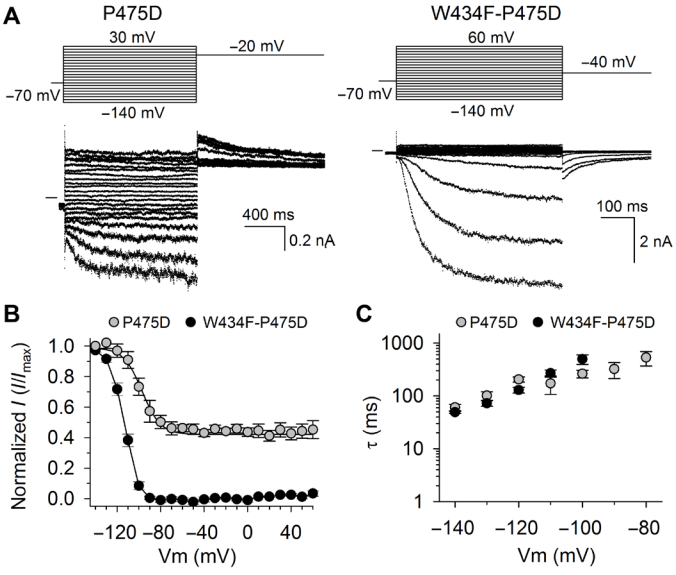

Fig. 2. Activation of the channel mutants Shaker-IR-P475D and Shaker-IR-W434F-P475D. (**A**) Representative whole-cell current recordings in Shaker-IR-P475D and Shaker-IR-W434F-P475D, acquired with the pulse protocols shown on top. Inward currents upon hyperpolarization were observed in both Shaker-IR-P475D and Shaker-IR-W434F-P475D. The horizontal bar at the start of the current traces indicates the zero-current level. (**B**) The normalized conducting current as a function of membrane potential obtained by analyzing the tail current amplitudes of Shaker-IR-P475D (gray circles; $N = 5$) and Shaker-IR-W434F-P475D (black circles; $N = 9$). V_{mid} was −99.1 ± 3.9 mV for Shaker-IR-P475D and −113.7 ± 0.4 mV for Shaker-IR-W434F-P475D. The solid lines represent the average fit with a Boltzmann charge-voltage function. (**C**) Time constants of elicited currents of Shaker-IR-P475D (gray circles; $N = 5$) and Shaker-IR-W434F-P475D (black circles; $N = 9$) shown in (A), obtained by fitting the onset of inward current with a single exponential function.

mutant channels, indicative of channels adopting a different partially closed state after the channels recover from their inactivated state (figs. S4 and S5).

The Shaker-IR-W434F-P475D is non-K^+ selective

K^+ selectivity of the mutant channels was verified by applying a strong hyperpolarizing pulse, to recover the channels from their inactivated state, followed by stepping the membrane potential to a range of different voltages (Fig. 3A). The peak tail current was plotted as a function of the applied membrane potential, which showed that Shaker-IR-P475D remained largely K^+ selective with a reversal potential (V_{rev}) of −60.8 ± 4.9 mV ($N = 4$) (Fig. 3B). K^+ selectivity was completely abolished in Shaker-IR-W434F-P475D, displaying a V_{rev} of approximately 0 mV ($N = 6$). To exclude that an alternative ion permeation pathway was created as is described for "omega" and "sigma" currents (*44*, *45*), well-established pore blockers were applied to prove that the currents recorded from Shaker-IR-W434F-P475D originated from ions flowing through the ion permeation pathway and the SF. Extracellular tetraethylammonium (TEA) is known to block ion permeation by binding to the pore mouth, and 100 mM TEA resulted in 62 ± 10% ($N = 6$) current reduction at −120 mV (Fig. 4). On the basis of the percentage current block, Shaker-IR-W434F-P475D displayed a TEA sensitivity that was slightly lower than what has been reported for WT Shaker-IR (*46*). Application of 500 μM flecainide, which is an intracellular pore blocker (*47*), resulted in 73 ± 13% ($N = 3$) current blockade, thereby providing further evidence that the recorded current was passing through the channel pore (Fig. 4). In addition, the gating modifier drug 4-aminopyridine (4-AP) that operates from the intracellular side of the pore (*48*, *49*) also blocked the inward current of Shaker-IR-W434F-P475D, whereby 10 mM resulted in 50 ± 6% ($N = 6$) current reduction (Fig. 4).

Current decay at depolarized membrane potentials has kinetics similar to those of C-type inactivation

After accumulating the ion channels in their conductive state, by applying either a strong depolarizing pulse (Shaker-IR) or a strong hyperpolarizing pulse (Shaker-IR-P475D and Shaker-IR-W434F-P475D), the kinetics of the subsequent decaying tail currents were analyzed. For WT Shaker-IR, deactivation is voltage dependent and accelerates with stronger repolarizing membrane potentials (Fig. 3C). For both mutant channels, however, largely voltage-independent time constants were obtained. The kinetics of Shaker-IR-P475D appeared to correspond to the inactivation kinetics of WT Shaker-IR channels displayed in fig. S6. The time constants for Shaker-IR-W434F-P475D were faster, which agrees with the notion that the W434F mutation accelerates the inactivation process. These data indicated that the decay of the tail currents for both Shaker-IR-P475D and Shaker-IR-W434F-P475D reflected on channels that inactivate. Because it is reported that the kinetics of inactivation slow down when the extracellular K^+ concentration increases, we tested whether this feature is preserved in the Shaker-IR-W434F-P475D mutant that lost its high K^+ selectivity (Fig. 3B). Increasing the extracellular K^+ concentration from 4 to 145 mM resulted in similar kinetics (fig. S7). This experimental result strongly supports the idea that the K^+ occupancy in the SF of Shaker-IR-W434F-P475D channels that recovered from their inactivated state notably differs from that of a WT SF that undergoes C-type inactivation.

Shaker-IR-W434F-P475D conducts $NMDG^+$

To capture the extent to which the SF is affected in Shaker-IR-W434F-P475D at negative membrane potentials, its ability to conduct ions larger than K^+ was tested by substituting monovalent cations in divalent cation free ICS and extracellular solutions (ECS) with *N*-methyl-D-glucamine ions ($NMDG^+$). Unexpectedly, macroscopic voltage- and time-dependent inward currents were observed at hyperpolarization (Fig. 5A). In addition, the kinetics of the hyperpolarization-induced currents were slowed (Fig. 5C). As these currents originate from channels recovering from inactivation upon AG reorganization at hyperpolarizing membrane potentials that normally close the AG, this slowing agrees with the presence of $NMDG^+$ that interferes with the conformational changes of the AG (*50*). In addition, to prove that the observed currents were carried by permeant $NMDG^+$ instead of protons, which cannot be excluded from the ICS and ECS, the pH of the ECS was varied to change the concentration gradient of H^+. When the intracellular $NMDG^+$ solution had a pH of 7.32 and the pH of the ECS was set at 6.52, 7.35, and 8.07, the equilibrium potential for H^+ shifts from −47.9 to −1.6 mV and 42.1 mV, respectively. However, V_{rev} was not influenced by different pH levels and remained at a value of around 0 mV in all three different ECS (fig. S8). This excludes the possibility that H^+ was the current carrier and strengthens the notion that Shaker-IR-W434F-P475D can conduct $NMDG^+$.

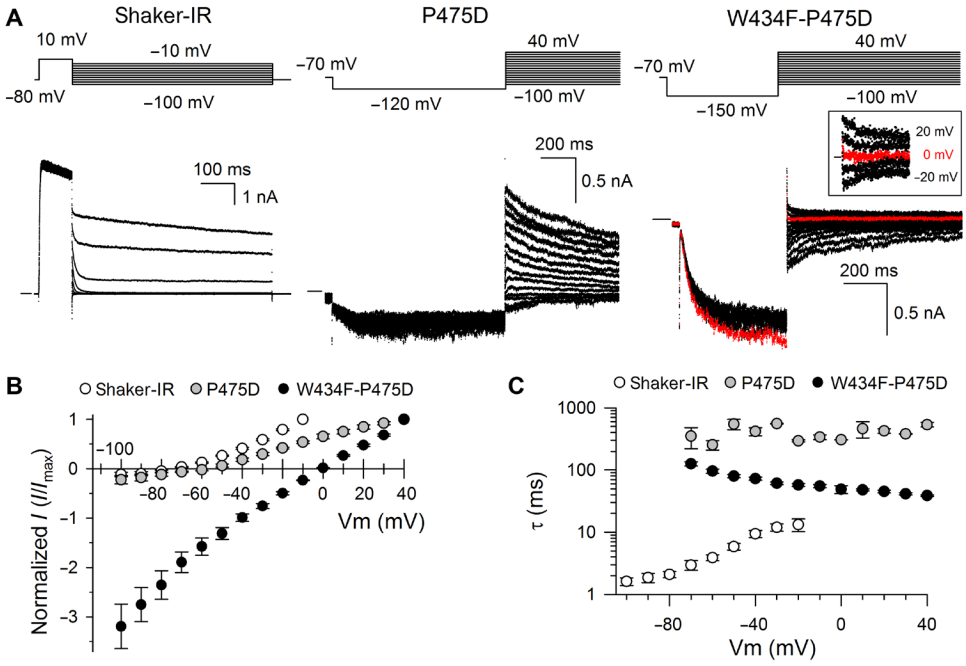

Fig. 3. Full activation of WT Shaker-IR and the mutant channels Shaker-IR-W434F-P475D and Shaker-IR-P475D. (**A**) Representative whole-cell current recordings in Shaker-IR, Shaker-IR-P475D, and Shaker-IR-W434F-P475D, elicited with a full-activation pulse protocol shown on top, to determine the ion selectivity of the channel. A horizontal bar at the beginning of the current traces indicates the zero-current level. The square inset displays the tail currents of Shaker-IR-W434F-P475D in more detail, from 20 to −20 mV, with the tail current elicited at 0 mV in red. (**B**) The normalized conducting current as a function of membrane potential obtained by analyzing the tail current amplitudes of Shaker-IR (white circles; $N = 5$), Shaker-IR-P475D (gray circles; $N = 4$), and Shaker-IR-W434F-P475D (black circles; $N = 6$). A similar V_{rev} was found for Shaker-IR (−76.5 ± 2.3 mV) and Shaker-IR-P475D (−60.8 ± 4.9 mV), while the V_{rev} of Shaker-IR-W434F-P475D displayed a large positive shift toward 0 mV. (**C**) Time constants of the decaying tail currents of Shaker-IR (white circles; $N = 5$), Shaker-IR-P475D (gray circles; $N = 4$), and Shaker-IR-W434F-P475D (black circles; $N = 6$), obtained by fitting the decaying tail currents elicited with the pulse protocols shown in (A).

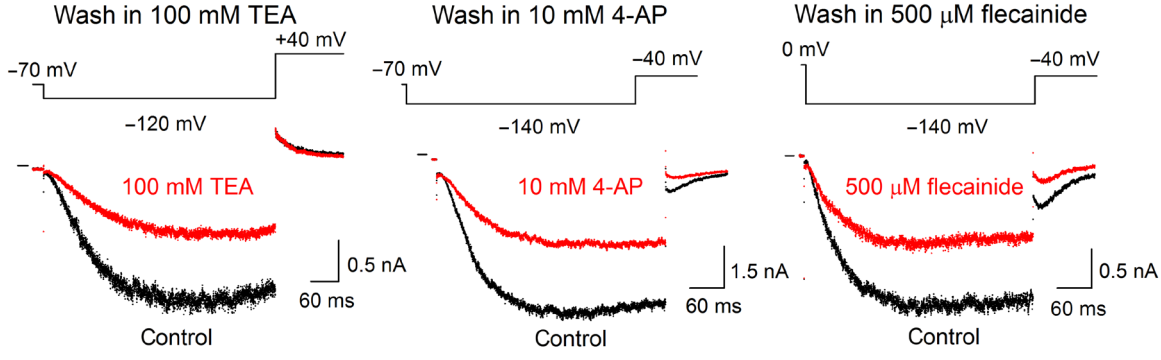

Fig. 4. Established pore blockers and 4-AP inhibit the Shaker-IR-W434F-P475D currents. TEA, 4-AP, and flecainide were used to prove that the observed nonselective currents recorded in standard ICS and extracellular solutions (ECS) pass through the ion-conducting pathway of the Shaker-IR-W434F-P475D channel. The black trace was recorded in control conditions, and the red trace displays steady-state inhibition (from left to right) by 100 mM TEA, 10 mM 4-AP, and 500 μM flecainide. The horizontal bar at the beginning of the whole-cell current recordings indicates the zero-current level. Currents were elicited using the pulse protocols shown on top.

T449V slows inactivation in Shaker-IR-W434F channels, revealing K^+ selective ionic currents

To evaluate whether the altered ion selectivity in Shaker-IR-W434F-P475D is due to the combination of a SF containing the W434F mutation and a channel's AG that did not fully close (P475D), the ion selectivity of a Shaker-IR-W434F variant that closes normally but displays slowed onset of inactivation was determined. To this end, the T449V mutation was introduced as it has been shown to reduce the speed of C-type inactivation (*51*). The Shaker-IR-T449V mutant yielded functional, voltage-gated ion channels that displayed a significant reduction of C-type inactivation (Fig. 6A). When combining the W434F mutation with T449V in Shaker-IR-W434F-T449V, ionic currents could be observed (Fig. 6A), albeit small and rapidly inactivating (fig. S9). Although there was no significant difference in the voltage dependency of channel activation between WT and Shaker-IR-T449V channels, the voltage dependency of Shaker-IR-W434F-T449V displayed a positive shift of approximately 11 mV (Fig. 6B). The voltage-dependent activation curve had a V_{mid} of

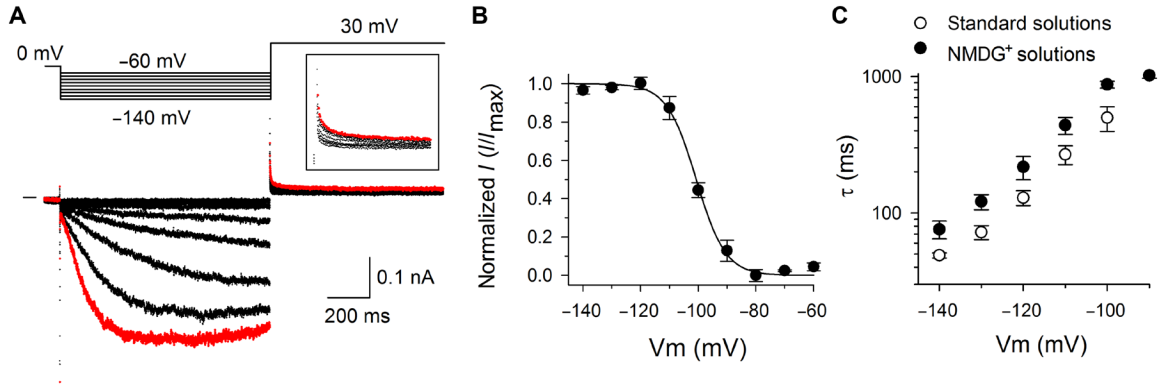

Fig. 5. Shaker-IR-W434F-P475D conducts $NMDG^+$. (**A**) Representative whole-cell current recordings in Shaker-IR-W434F-P475D, elicited with the pulse protocol on top, using ICS and ECS that contained no divalent cations and with the monovalent cations replaced by $NMDG^+$. The square inset displays the tail currents in more detail. (**B**) Conductance versus voltage relation obtained in $NMDG^+$ solutions ($N = 5$). The solid line represents the average fit with a Boltzmann charge-voltage function. (**C**) Time constants of hyperpolarization-induced current increases in standard solutions (white circles; $N = 6$) and $NMDG^+$ solutions (black circles; $N = 5$). Note that $NMDG^+$ slowed down the time constants.

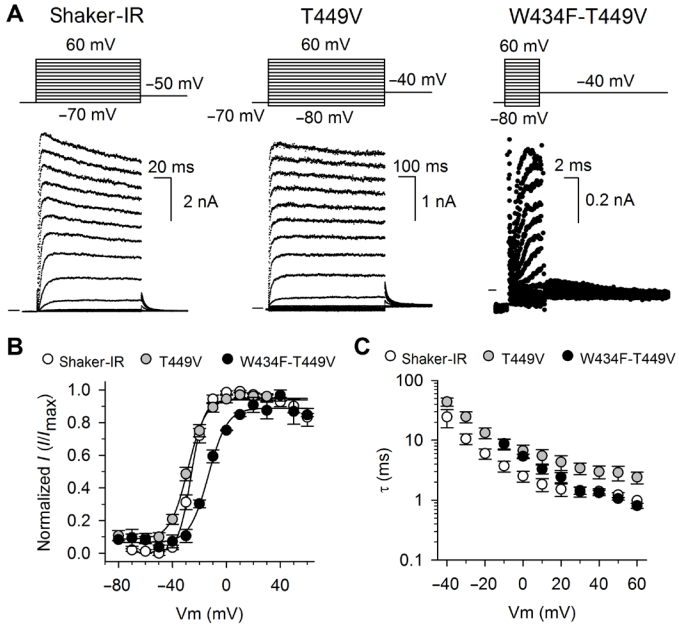

Fig. 6. Activation of WT Shaker-IR and the mutant channels Shaker-IR-T449V and Shaker-IR-W434F-T449V. (**A**) Representative whole-cell current recordings from Shaker-IR, Shaker-IR-T449V, and Shaker-IR-W434F-T449V, acquired with the activation protocol shown on top. A horizontal bar at the beginning of the current traces indicates the zero-current level. (**B**) The normalized conducting current as a function of membrane potential obtained by analyzing the tail current amplitudes of Shaker-IR (white circles; $N = 4$), Shaker-IR-T449V (gray circles; $N = 10$), and Shaker-IR-T449V-W434F (black circles; $N = 3$). V_{mid} was −25.2 ± 1.5 mV for WT Shaker-IR, −27.8 ± 1.4 mV for Shaker-IR-T449V, and −15.3 ± 3.1 mV for Shaker-IR-W434F-T449V. (**C**) Time constants of activation, obtained by fitting the onset of activation with a single exponential function, of Shaker-IR (white circles; $N = 4$), Shaker-IR-T449V (gray circles; $N = 5$), and Shaker-IR-T449V-W434F (black circles; $N = 10$).

−15.3 ± 3.1 mV ($N = 3$), while for Shaker-IR and Shaker-IR-T449V, V_{mid} equaled to −25.2 ± 1.5 ($N = 4$) and −27.8 ± 1.4 mV ($N = 10$), respectively. The kinetics of channel activation and deactivation were slowed down in both Shaker-IR-T449V and Shaker-IR-W434F-T449V (Figs. 6C and 7C). The K^+ selectivity was largely preserved in the Shaker-IR-W434F-T449V channel, displaying a V_{rev} of −64.0 ± 2.4 mV ($N = 7$) compared to a V_{rev} of −76.5 ± 2.3 mV in Shaker-IR ($N = 5$) and −76.8 ± 1.7 mV ($N = 7$) in Shaker-IR-T449V (Fig. 7B). This result indicates that, when the AG closes completely, the W434F-containing SF adopts a K^+ selective conformation. To exclude that the T449V mutation rescued the W434F-mutant SF and restored it to the WT phenotype, the triple-mutant Shaker-IR-W434F-T449V-P474D channel was evaluated. This triple mutant behaved similarly to Shaker-IR-W434F-P474D, and upon recovery from inactivation, the K^+ selectivity was lost (fig. S10). This indicates that the T449V mutant does not rescue the inactivated state of the W434F-mutant SF in a Shaker-IR-P474D background.

Three-dimensional structure of W67F KcsA mutant with a closed AG

Consequently, when the AG can close completely, the W434F mutant's SF adopts a K^+ selective conformation that most likely resembles a conductive SF in WT Shaker-IR channels. To gain structural insights into the conformation of the W434F mutant channel's SF, when its AG is in the closed conformation, we took a backdoor strategy and crystallized the equivalent mutation in the bacterial KcsA (K channel of Streptomyces A) K^+ channel, namely, the W67F KcsA mutant channel. We turned to the voltage-independent K^+ channel KcsA because, at 0 mV, the Shaker-IR channel's AG is open (Fig. 6B), and its structure cannot be solved with a closed AG. The KcsA-W67F mutant with the AG closed was crystallized as a complex with an antibody fragment that facilitates crystal formation. The KcsA-Fab complex crystallized in the *I*4 space group and diffracted x-rays to 3.2 Å (table S1). At this resolution, the overall architecture of the channel remained similar to WT KcsA (Fig. 8). A structural alignment of the W67F and the WT KcsA pore helices and SFs (with their AGs in the closed state) showed that their overall structure is similar (root mean square deviation of 0.33 Å for the SF atoms), with few structural changes. The most noticeable changes detected in the W67F mutant structure involve the following: (i) a change in atomic position of the aromatic cuff residues, (ii) a presumably increase in the disorder of the E71 side chain that precluded its modeling in the final structural model, and (iii) a change in the position of the G77 carbonyl group that turns it away from the

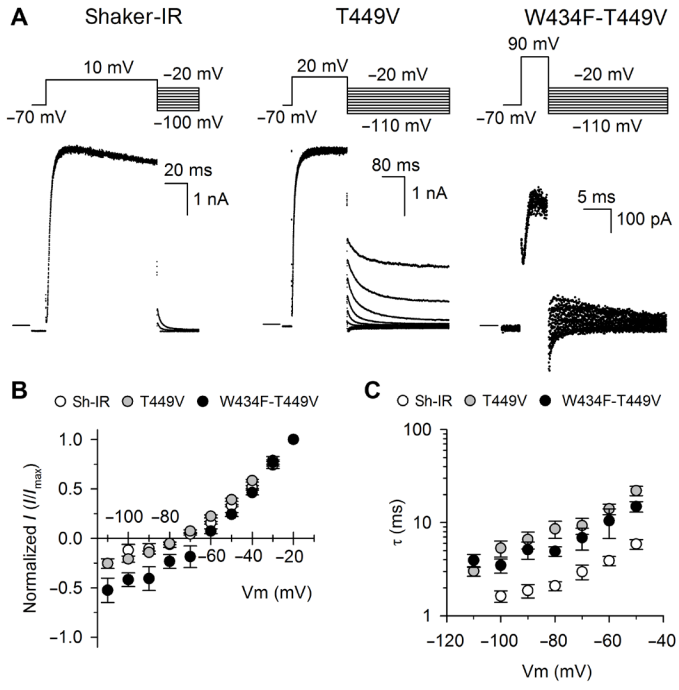

Fig. 7. Ion selectivity and deactivation kinetics of WT Shaker-IR and the mutant channels Shaker-IR-W434F-P475D and Shaker-IR-P475D. (**A**) Representative whole-cell current recordings in Shaker-IR, Shaker-IR-T449V, and Shaker-IR-W434F-T449V, acquired using the full activation protocol shown on top. The zero-current level is indicated by a horizontal bar at the beginning of the current traces. (**B**) The normalized conducting current as a function of membrane potential obtained by analyzing the tail current amplitudes of Shaker-IR (white circles; $N = 5$), Shaker-IR-T449V (gray circles; $N = 7$), and Shaker-IR-W434F-T449V (black circles; $N = 7$). This shows that all three channels have a similar degree of K^+ selectivity with a V_{rev} of −76.5 ± 2.3 mV for Shaker-IR, −76.8 ± 1.7 mV, for Shaker-IR-T449V and −64.0 ± 2.4 mV for Shaker-IR-W434F-T449V. (**C**) Time constants of deactivation of Shaker-IR (white circles; $N = 5$), Shaker-IR-T449V (gray circles; $N = 7$), and Shaker-IR-W434F-T449V (black circles; $N = 7$), obtained by fitting the deactivating tail currents with a single exponential function.

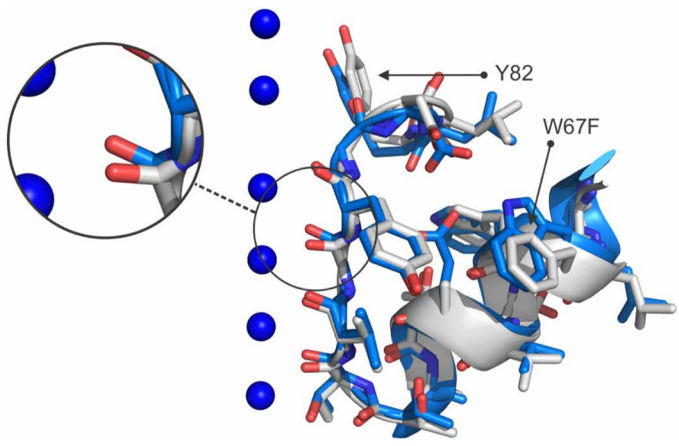

Fig. 8. Crystal structure of the KcsA-W67F mutant and WT KcsA pore helix and SF. A structural alignment superimposing the WT KcsA (light blue sticks) and the KcsA-W67F mutant (yellow sticks) pore helix and SF is shown. The amino acid side chains of the Tyr^{82} and the phenylalanine substitution at the position 67 are indicated with black arrows to highlight the structural changes at the aromatic cuff caused by the W67F mutant. On the left, an inset zooming at the G77 carbonyl group highlights its structural changes, which underlies the ion vacancy at the second ion binding site.

central axis of symmetry. Focusing on the K^+ occupancy in the SF, an aggregate of three bound K^+ were observed (Fig. 9). Ions at the first, third, and fourth binding sites were observed with reduced ion occupancy or a vacancy at the second ion binding site. This reduced ion occupancy seems the consequence of changes at the G77 carbonyl group. Nevertheless, a SF with three bound K^+ has been shown to be highly K^+ selective (*5*, *18*, *27*, *30*, *52*, *53*). Given the high structural similarities between the SF of Kv channels and KcsA, the SF structure of the KcsA-W67F mutant channel presented here supports the idea that, in the closed conformation, after recovering from C-type inactivation, the Shaker-IR channel harboring the W434F mutant with a closed AG adopts a conductive and K^+ selective SF conformation. However, the W434F-mutant SF in the open and inactivated conformation, contrary to the Shaker-IR WT SF, adopts a wider and non-K^+ selective conformation.

DISCUSSION

C-type inactivation in Kv channels develops upon prolonged channel activation and is modulated by external K^+, where elevated concentrations slow down C-type inactivation (*51*, *54*). In addition, extracellular TEA also slows down C-type inactivation (*55*, *56*). These observations imply that C-type inactivation is associated with rearrangements in the outer pore region, typically interpreted as a constriction of the permeation pathway that prevents ion conduction (*16*–*18*, *57*, *58*). Some C-type inactivated channels are able to conduct Na^+ in the absence of K^+ (in nonphysiologically relevant conditions) (*38*), which demonstrates that conformational changes take place in the SF. Similarly, Na^+ currents in the absence of K^+ have been observed in the Shaker-IR-W434F mutant channel (*39*). Moreover, in recent years, it has also been implied that the abolished or reduced ion conduction of C-type inactivated channels results from a small dilation of the SF rather than a constriction (*59*). Here, we further investigated the ion selectivity of W434F-containing Shaker-IR channels when the SF recovers from its inactivated state at hyperpolarized cell membrane potentials that normally will cause AG closure.

The P475 residue in Shaker is the second proline of the PVP motif, a region that has been proposed to form a gating hinge in Kv channels (*12*). Substituting this residue with an aspartate (P475D) converted Shaker-IR into a constitutive conductive channel (Fig. 1), as reported previously (*40*, *41*). Compared to previous reports of the Shaker-IR-P475D mutant, we were interested in studying recovery from inactivation, and the main difference with those reports is the use of a more positive holding potential that promotes channel inactivation during the interpulse time. Subsequently, time- and voltage-dependent currents were recorded at hyperpolarizing negative potentials when the channels recover from a lower or nonconductive (inactivated) state. Next, we set out to record ionic currents in Shaker-IR-W434F-P475D during hyperpolarization, when the SF recovers from inactivation while the AG is deactivating but unable to close completely. As expected, time- and voltage-dependent currents were observed at negative membrane potentials in Shaker-IR-W434F-P475D (Fig. 2A). Oppositely, the decay of the tail currents, elicited during depolarizing voltage steps upon a negative prepulse (Fig. 3A), reflects the onset of channel inactivation (fig. S1). Accordingly, the

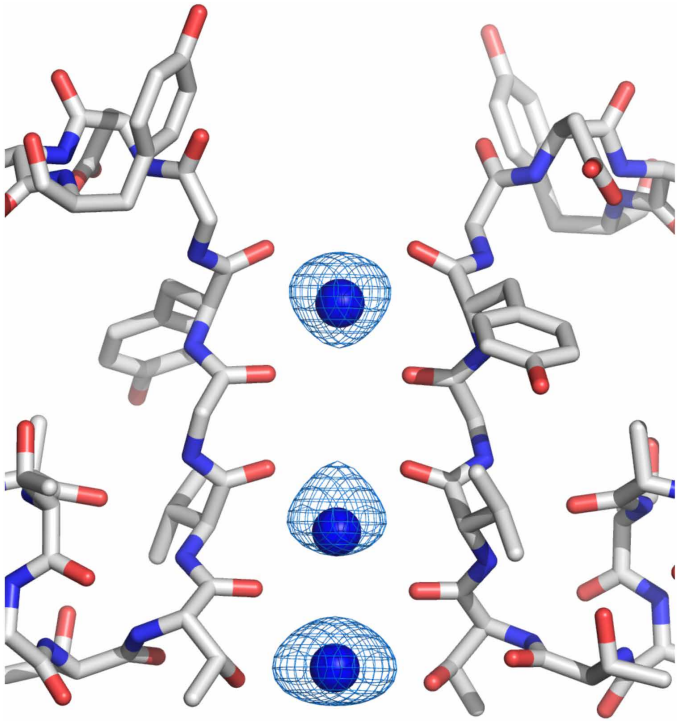

Fig. 9. Ion occupancy in the SF of the KcsA-W67F mutant with its AG closed. The SF of the KcsA-W67F mutant in the closed conformation displaying only two diagonal subunits for clarity. The Fo-Fc electron density map is displayed in light blue mesh (contoured at 7σ), validating the ions bound to the channel's SF. Ions were bound at the first, third, and fourth K^+ binding sites. The W67F's SF remains conductive and adopted a WT-like structure, albeit with no or reduced K^+ occupancy at the second binding site.

obtained time constants were largely voltage independent, a typical hallmark of C-type inactivation in WT channels (Fig. 3C). In contrast to Shaker-IR-W434F that does not display ionic currents, the inactivation of the Shaker-IR-W434F-P475D is not ultrafast, and ionic tail currents could be observed. A possible explanation is that the W434F inactivates from a SF filter that is stabilized in an intermediate recovering state due to the P475D mutation, as depicted in fig. S1. Nevertheless, compared to Shaker-IR-P475D, the obtained time constants were 10-fold faster in the Shaker-IR-W434F-P475D, in agreement with the W434F mutation accelerating inactivation (*37*). Comparing the inactivation time constants of Shaker-IR-P475D with those of Shaker-IR (fig. S6), the P475D mutation on its own appeared to accelerate the inactivation process slightly, which is expected if the AG and SF are allosterically coupled and the SF is stabilized in an intermediate state because of the incomplete AG closure (fig. S1) (*25*–*29*). However, caution is advised because the P475D mutant could cause extra conformational changes to the channel protein that prevents the full closure of the AG. Nevertheless, by making the closed state conductive, we recorded currents through both a WT SF (Shaker-IR-P475D) and a W434F-containing SF (Shaker-IR-W434F-P475D) when the SF was recovering from the inactivated state. Apparently, during this recovery process, the W434F-containing SF adopted a conductive conformation that lost its characteristic high K^+ selectivity (Fig. 3B). Moreover, the Shaker-IR-W434F-P475D mutant was conductive to the large and normally impermeable $NMDG^+$ (Fig. 5). This was not the case for Shaker-IR-P475D, indicating that the altered ion selectivity was brought about by the introduction of the W434F mutation. Although we cannot exclude that this loss in K^+ selectivity is brought about by conformational changes of the P475D mutant that exacerbate the W434F mutation, our data show that, within the same channel background, a W434F-containing SF adopts a different C-type inactivated state.

As C-type inactivation is associated with rearrangements in the outer pore region, mutations at the extracellularly located pore residue T449 in Shaker-IR can accelerate (T449E, T449K, and T449A) and decelerate (T449H, T449Y, and T449V) this process (*51*). Addition of the T449V mutation in Shaker-IR-W434F slowed down C-type inactivation such that ionic currents could be recorded from a W434F-containing SF when the AG gate was closed completely and opens upon membrane depolarization (Fig. 6). This Shaker-IR-W434F-T449V channel displayed small and rapidly inactivating currents, which agrees with a filter that is prone to inactivate (Fig. 6 and fig. S8). The activation kinetics were similar to those of WT Shaker-IR and Shaker-IR-T449V channels, but the voltage dependence of channel activation was slightly shifted toward more positive potentials. However, in contrast to the ion selectivity of the conducting Shaker-IR-W434F-P475D channels, the currents of the Shaker-IR-W434F-T449V were K^+ selective. This strongly suggests that, when the AG closes completely, the W434F-containing SF adopts a highly K^+ selective conformation that most likely resembles a conductive SF in the WT Shaker-IR channels. Because the Shaker-IR channel at 0 mV will have an open AG, we turned to the KcsA K^+ channel to gain structural insights into the closed W434F mutant channel's SF by crystallizing the equivalent KcsA W67F mutant with a closed AG. A plausible technical limitation of using KcsA in this study is the lack of a VSD. It has been shown that a direct communication between the VSD and the pore domain (including the SF) is known to regulate the C-type inactivation process in Kv channels (*33*). However, the onset of C-type inactivation occurs when the VSDs are activated, which is the case for Shaker-IR at 0 mV. In contrast, upon hyperpolarization, the VSDs are in the down or deactivated state, which triggers AG closure, and consequently, the SF is presumably in the conductive conformation. For these reasons, we reasoned that the closed KcsA-W67F structure represents a good structural surrogate for a K^+ channel pore domain with its AG closed and the SF in the conductive state. The structure of the W67F mutant showed a WT-like SF with three bound K^+ at the first, third, and fourth binding sites (Fig. 9). We and others have demonstrated that, in KcsA and other K^+ channels, a SF with three bound K^+ remains fully K^+ selective (*5*, *18*, *27*, *30*, *52*, *53*). Resolving the structure of KcsA-W67F in the closed conformation but in the presence of 10 mM TBA (Tetrabutylammonium) showed a conductive SF but an aggregate of four bound K^+ (*60*). We attribute the reason for this incongruence with our structure to the presence of TBA. Whereas TBA does not seem to affect the ion occupancy of the KcsA WT SF (*61*), an effect on the W67F-mutant SF cannot be ruled out (*60*). Regardless of this difference, both structures display a conductive SF, which agrees with the notion that a Shaker-IR-W434F channel with its AG closed contains a conductive and K^+ selective filter.

$NMDG^+$ conduction has been reported previously in open Kv3.1 and Kv3.2b channels and in mutant Kv1.5 channels, demonstrating the flexibility of the SF (*62*). A key residue in introducing this flexibility in Kv3.1 channels appeared the tyrosine residue Y407 (Kv3.1 numbering), which is the equivalent to T449 in Shaker-IR channels (*51*). Similarly, mutating only one conserved glycine residue (G347)

in the neuronal P2X4 resulted in the same flexibility, allowing $NMDG^+$ conduction (*63*). In the absence of K^+ ions, Loboda *et al.* (*64*) reported that the Shaker-IR and the W434F mutant displayed permeability to large cations as they transition to a dilated state, which is reminiscent of the increased $NMDG^+$ permeability shown by the Shaker-IR-W434F-P475D mutant (Fig. 5). However, the Shaker-IR-P475D did not show increased $NMDG^+$ permeability, which reinforces the idea that the SF structure of the W434F mutant represents a nonphysiological C-type inactivated state with altered ion selectivity. It seems that this nonphysiologically relevant "inactive state" of the Shaker channels can be achieved by dekalifying the channel or by introducing the W434F mutant.

The recently reported cryo–electron microscopy (cryo-EM) structure of the Shaker-IR-W434F channel shows a clear widening of the outermost K^+ binding sites (*34*), which strongly suggests that a widening or dilation of W434F's SF underlies the nonconductive phenotype of this mutant channel. This structure of the Shaker-IR-W434F SF can be reconciled with the lack of K^+ over Na^+ selectivity and can explain the $NMDG^+$ conductance displayed by our Shaker-IR-W434F-P475D mutant when recovering from inactivation. On the other hand, the Shaker-IR-P475D channels harboring a WT SF remained highly K^+ selective and impermeable to $NMDG^+$ when recovering from their C-type inactivated state. Therefore, the W434F-mutant SF most likely does not resemble a Shaker-IR WT C-type inactivated SF. Possibly, by accelerating the inactivation process, the W434F mutation promotes a nonphysiologically relevant deep inactivated state. The cryo-EM structures of the Shaker-IR and the Shaker-IR-W434F channels, both obtained at 0 mV and under similar conditions (*34*), displayed significantly different SF structures, in which the activated Shaker-IR SF shows an aggregate of four bound K^+ ions and no discernible widening of the SF. This agrees with our experimental findings and our conclusion of a nonequivalence between an inactivated WT and an inactivated W434F-mutant SF.

In conclusion, combining the W434F with the P475D mutation converts the depolarization-activated and K^+ selective Shaker-IR channel into a nonselective, hyperpolarization conductive cation channel. Most unexpectedly, this Shaker-IR-W434F-P475D mutant channel allowed permeation of the large $NMDG^+$ ions, suggesting a widening or dilation of the W434F-containing SF during recovery of inactivation. When the AG can close normally, such as in Shaker-IR-W434F-T449V, K^+ selectivity is restored. The structure of the KcsA-W67F mutant channel with the AG closed, which is the equivalent to the W434F Shaker mutant channel, showed that, in the closed state, the W434F's SF resembles a K^+ selective conformation. Because the Shaker-IR-P475D remains highly K^+ selective, the SF conformations during recovery from the C-type inactivated state differs between the W434F-containing mutant and WT Shaker-IR channels. Thus, our experimental results strongly suggest that the naturally occurring Shaker-IR C-type inactivated state and the W434F-mutant inactivated state are not functional and likely structural equivalents.

MATERIALS AND METHODS

Creating the Shaker-IR W434F, T449V, and P475D channel mutants

Shaker-IR complementary DNA (cDNA) was cloned in the GW1-CMV vector for expression in mammalian cells. W434F, T449V, and P475D mutations were introduced through site-directed mutagenesis using the QuikChange site-directed mutagenesis kit (Agilent, CA, USA) and custom-designed primers that contain the desired mutation (Integrated DNA technologies, IA, USA). Plasmid DNA was amplified in XL2-blue ultracompetent *Escherichia coli* (Agilent Technologies, CA, USA) and purified using the NucleoBond Xtra Maxi kit (Machery-Nagel, Düren, Germany). Sanger sequencing of the constructs, performed by the VIB genetic sequencing facility (VIB Genomics Core, Antwerp, Belgium), confirmed successful mutagenesis.

Cell culture, transfection, and electrophysiology

WT Shaker-IR, Shaker-IR-P475D, and Shaker-IR-W434F-P475D channels were transiently expressed in HEK293 cells by transfecting subconfluent cell culture dishes of 35 mm with 20 ng and 5 μg of plasmid cDNA, respectively, using Lipofectamine 2000 (Thermo Fisher Scientific, MA, USA). A similar approach was used for Shaker-IR-T449V and Shaker-IR-W434F-T449V, but Ltk^- cells were used. Cells were incubated at 37°C under 5% CO_2 and collected 24 hours after transfection using Gibco 0.05% trypsin-EDTA (Thermo Fisher Scientific). Cells transfected with Shaker-IR-W434F-T449V were incubated for 48 hours followed by a 3-hour incubation at 25°C before collection to increase ion channel expression. Whole-cell ionic current experiments were performed at room temperature (20°C) using an Axopatch 200b amplifier, and recordings were digitized with the Digidata 1440 data acquisition system (Molecular Devices, CA, USA). Recordings were sampled at 2 to 10 kHz after passing a 1- to 5-kHz low-pass filter. Voltage errors were minimized using series resistance compensation of up to 80%. If the voltage error estimate exceeded 5 mV after series resistance compensation, then the experiments were excluded from analysis. Capacitive currents were minimized using capacitance compensation of up to 80%. Recordings were not corrected for leak and capacitance using an opposite pulse protocol (–*P*/4 subtraction).

Cells were continuously superfused with standard ECS: 130 mM NaCl, 4 mM KCl, 1.8 mM $CaCl_2$, 1 mM $MgCl_2$, 10 mM Hepes, and 10 mM glucose, adjusted to pH 7.35 with NaOH. ECS with pH 8.07 and 6.52 were obtained by titration using NaOH or HCl, respectively. Patch pipettes were pulled from 1.2-mm borosilicate glass (World Precision Instruments, FL, USA) with a P-2000 puller (Sutter Instruments, CA, USA) and afterward heat-polished, resulting in pipette resistances of 1 to 2 megohm. The pipettes were filled with standard ICS: 110 mM KCl, 1 mM NaCl, 5 mM K_4BAPTA, 5 mM K_2ATP, 1 mM $MgCl_2$, and 10 mM Hepes and adjusted to pH 7.2 with KOH. To replace the monovalent cations in the solutions, $NMDG^+$ was used. The ECS contained 140 mM $NMDG^+$, 10 mM Hepes, and 10 mM glucose, titrated to pH 7.35 with HCl. The ICS contained 140 mM $NMDG^+$, 10 mM Hepes, and 10 mM EGTA, titrated to pH 7.2 with HCl. The compounds, 4-AP, flecainide, and TEA, were dissolved in the ECS. Switching of ECS and application of compound solutions in the vicinity of the patched cell were achieved using a pressurized fast perfusion system (custom built with electrofluidic valves purchased from Lee Products Ltd., Buckinghamshire, UK) and a quartz micromanifold (ALA Scientific, Farmingdale, NY, USA), allowing rapid exchange of the external solutions. Before the sealing process, the junction potentials were zeroed with the filled pipette in the bath solution. Applied pulse protocols are shown in the figures.

Data analysis

Data were excluded from analysis when the voltage error estimate exceeded 5 mV after series resistance compensation. Data analysis

was performed with pCLAMP 10 software (Molecular Devices) and Microsoft Excel (Microsoft, NM, USA), and figures were constructed in SigmaPlot 11 (Systat Software, CA, USA). The voltage dependency of channel activation and inactivation was analyzed by plotting the normalized peak tail currents in function of the preceding membrane potential. The *I-V* curves from the decaying tail current data, which reveals the reversal membrane potential, were obtained by plotting the normalized peak tail current in function of the applied potential. Note that only 3 of 13 cells expressing Shaker-IR-W434F-T449V displayed large enough tail currents at −40 mV following activation to include for the analysis of the voltage dependency of activation. All *I-V* curves were fitted with a single Boltzmann equation: $y = 1/(1 + \exp[-(V - V_{1/2})/k])$, with V as the applied voltage, $V_{1/2}$ as the voltage at which half of the channels are opened or inactivated, and k as the slope factor. Time constants of activation for Shaker-IR and Shaker-IR-W434F-T449V were obtained by fitting the increase in current amplitude after the sigmoidal delay with a single exponential function. Time constants for recovery from inactivation for the P475D mutants were obtained by fitting the hyperpolarized-induced current increase with a single exponential function. The time constants of inactivation and deactivation were obtained by fitting the decay of tail current recordings with a single-exponential function. Each current trace was fitted individually, and the goodness of the fit was evaluated on the basis of the difference plots. All data are represented as mean values ± SEM, with N as the number of cells analyzed.

KcsA-W67T protein expression and purification

The KcsA-closed W67F cloned in the expression plasmid pQE70 was transformed in the *E. coli* XL10-Gold (Agilent, CA, USA) and grown overnight in LB medium with the following additive composition: 1% glucose and 0.4 mg/ml ampicillin at 37°C. The next day, 10 ml of the overnight culture was added to a fresh 1 liter of LB medium complemented with 0.2% glucose, ampicillin (0.4 mg/ml), 0.5% glycerol, and 5 mM $MgCl_2$ (*65*) and cultured at 37°C at 250 rpm until it reached ~0.6 optical density at 600 nm. Next, the temperature of the cultures was dropped to 29°C under continuous shaking for 60 min. At this moment, protein expression was started by adding 0.1 mM isopropyl-β-D-thiogalactopyranoside, and the medium was supplemented with 10 mM $BaCl_2$ (a known blocker of potassium channels) and ampicillin (0.4 mg/ml) to maintain the expression vector selection. The protein expression took place overnight at 29°C. Twenty-four hours later, the cells were harvested by centrifugation at 4600 rpm at 4°C. The collected cells expressing the W67F mutant were resuspended in solubilization [TKS buffer: 50 mM tris-HCl and 150 mM KCl (pH 8.0)] supplemented with protease inhibitors and treated with egg lysozyme (1 mg/ml) and rotated at room temperature for 1 hour. The cell suspension was broken by passing it through a microfluidizer and then spun down at 100,000*g* for 1 hour to pellet the cell membranes. The cell membranes were resuspended in TKS buffer supplemented with protease inhibitors, and aliquots were stored at −80°C until further use. KcsA was extracted from the *E. coli* membrane by adding 20 mM dodecyl maltoside (DDM), 10% glycerol, asolectin (0.1 mg/ml), and protease inhibitors for 2 hours at 4°C. The solubilized W67F mutant channels were fractionated from the insoluble material by centrifugation at 100,000*g*. Next, the supernatant was applied to a TALON resin column (Clontech, CA, USA), which was washed with TKS buffer supplemented with 15 mM imidazole and 2 mM DDM, 5% glycerol, and asolectin (0.1 mg/ml). The protein was eluted by applying TKS buffer supplemented with 400 mM imidazole and 2 mM DDM, 5% glycerol, and asolectin (0.1 mg/ml). The pure protein was concentrated, incubated with chymotrypsin (1:50) for 2 hours at room temperature, and applied to a size exclusion chromatography column ENrich SEC 650 10 × 300 column (Bio-Rad, CA, USA) for final purification and to determine whether the purified channel was properly folded.

Macromolecular crystallography

C-terminal truncated KcsA W67F mutants in TKS buffer supplemented with 2 mM DDM, asolectin (0.1 mg/ml), and 2% glycerol were mixed with an antibody fragment needed for the crystallization process. The channel-Fab complex was purified by passing it through a size exclusion chromatography column ENrich SEC 650 10 × 300 column (Bio-Rad) preloaded with TKS buffer + 0.5 mM DDM + asolectin (0.1 mg/ml). Crystallization was performed by the sitting drop method in 22 to 26% PEG-400 (polyethylene glycol, molecular weight 400) (v/v), 50 mM magnesium acetate, and 50 mM sodium acetate (pH 4.8. to pH 5.4) at 19°C. Crystals appeared within a week, and they were immediately cryo-protected by increasing the concentration of PEG-400 to 40%. A dataset was acquired from a single crystal for the W67F mutant at the beamline 14-1, at the Stanford Synchrotron Radiation Laboratory. Image processing and data reduction were performed with HKL-2000 (*66*).

Crystal structure determination

The structures of the closed state of the KcsA-W67F in 300 mM KCl [Protein Data Bank (PDB), 7SQW] were solved by molecular replacement using the atomic model of the antibody fragment from a KcsA-Fab complex structure at 2-Å resolution (PDB, 1K4C) (*67*) as the search model. The three-dimensional model for the W67F mutant channels were made by using Coot (*68*) and were refined with Phenix (*69*). The protocol for refining these structures included 2 to 5 cycles of rigid body, energy minimization, simulated annealing, and individual B-factor refinements. Table S1 contains the statistics of the crystallographic W67F data analysis. The crystal structural figures of the W67F used here were made using PyMOL (https://pymol.org).

SUPPLEMENTARY MATERIALS

Supplementary material for this article is available at https://science.org/doi/10.1126/sciadv.abn1731

View/request a protocol for this paper from *Bio-protocol*.

REFERENCES AND NOTES

1. B. Hille, *Ion Channels of Excitable Membranes* (Sinauer Associates Inc., ed. 3, 2001).
2. D. Fedida, J. C. Hesketh, Gating of voltage-dependent potassium channels. *Prog. Biophys. Mol. Biol.* **75**, 165–199 (2001).
3. R. MacKinnon, Determination of the subunit stoichiometry of a voltage-activated potassium channel. *Nature* **350**, 232–235 (1991).
4. S. B. Long, E. B. Campbell, R. Mackinnon, Crystal structure of a mammalian voltage-dependent *Shaker* family K^+ channel. *Science* **309**, 897–903 (2005).
5. D. A. Doyle, J. Morais Cabral, R. A. Pfuetzner, A. Kuo, J. M. Gulbis, S. L. Cohen, B. T. Chait, R. MacKinnon, The structure of the potassium channel: Molecular basis of K^+ conduction and selectivity. *Science* **280**, 69–77 (1998).
6. A. J. Labro, D. J. Snyders, Being flexible: The voltage-controllable activation gate of kv channels. *Front. Pharmacol.* **3**, 168 (2012).
7. R. Blunck, J. F. Cordero-Morales, L. G. Cuello, E. Perozo, F. Bezanilla, Detection of the opening of the bundle crossing in KcsA with fluorescence lifetime spectroscopy reveals the existence of two gates for ion conduction. *J. Gen. Physiol.* **128**, 569–581 (2006).
8. R. Blunck, Z. Batulan, Mechanism of electromechanical coupling in voltage-gated potassium channels. *Front. Pharmacol.* **3**, 166 (2012).

9. T. Kalstrup, R. Blunck, Dynamics of internal pore opening in K(V) channels probed by a fluorescent unnatural amino acid. *Proc. Natl. Acad. Sci. U.S.A.* **110**, 8272–8277 (2013).
10. D. del Camino, M. Holmgren, Y. Liu, G. Yellen, Blocker protection in the pore of a voltage-gated K^+ channel and its structural implications. *Nature* **403**, 321–325 (2000).
11. J. N. Bright, I. H. Shrivastava, F. S. Cordes, M. S. P. Sansom, Conformational dynamics of helix S6 from Shaker potassium channel: Simulation studies. *Biopolymers* **64**, 303–313 (2002).
12. A. J. Labro, A. L. Raes, I. Bellens, N. Ottschytsch, D. J. Snyders, Gating of Shaker-type channels requires the flexibility of S6 caused by prolines. *J. Biol. Chem.* **278**, 50724–50731 (2003).
13. D. del Camino, G. Yellen, Tight steric closure at the intracellular activation gate of a voltage-gated K^+ channel. *Neuron* **32**, 649–656 (2001).
14. D. P. Tieleman, I. H. Shrivastava, M. R. Ulmschneider, M. S. Sansom, Proline-induced hinges in transmembrane helices: Possible roles in ion channel gating. *Proteins* **44**, 63–72 (2001).
15. T. Hoshi, W. N. Zagotta, R. W. Aldrich, Two types of inactivation in Shaker K^+ channels: Effects of alterations in the carboxy-terminal region. *Neuron* **7**, 547–556 (1991).
16. Y. Liu, M. E. Jurman, G. Yellen, Dynamic rearrangement of the outer mouth of a K^+ channel during gating. *Neuron* **16**, 859–867 (1996).
17. J. F. Cordero-Morales, L. G. Cuello, Y. Zhao, V. Jogini, D. M. Cortes, B. Roux, E. Perozo, Molecular determinants of gating at the potassium-channel selectivity filter. *Nat. Struct. Mol. Biol.* **13**, 311–318 (2006).
18. L. G. Cuello, V. Jogini, D. M. Cortes, E. Perozo, Structural mechanism of C-type inactivation in K^+ channels. *Nature* **466**, 203–208 (2010).
19. V. Pau, Y. Zhou, Y. Ramu, Y. Xu, Z. Lu, Crystal structure of an inactivated mutant mammalian voltage-gated K^+ channel. *Nat. Struct. Mol. Biol.* **24**, 857–865 (2017).
20. J. Li, J. Ostmeyer, L. G. Cuello, E. Perozo, B. Roux, Rapid constriction of the selectivity filter underlies C-type inactivation in the KcsA potassium channel. *J. Gen. Physiol.* **150**, 1408–1420 (2018).
21. L. G. Cuello, D. M. Cortes, E. Perozo, The gating cycle of a K^+ channel at atomic resolution. *eLife* **6**, e28032 (2017).
22. T. G. Szanto, F. Zakany, F. Papp, Z. Varga, C. J. Deutsch, G. Panyi, The activation gate controls steady-state inactivation and recovery from inactivation in *Shaker*. *J. Gen. Physiol.* **152**, e202012591 (2020).
23. M. L. Chapman, H. M. VanDongen, A. M. VanDongen, Activation-dependent subconductance levels in the drk1 K channel suggest a subunit basis for ion permeation and gating. *Biophys. J.* **72**, 708–719 (1997).
24. A. M. J. VanDongen, K channel gating by an affinity-switching selectivity filter. *Proc. Natl. Acad. Sci. U.S.A.* **101**, 3248–3252 (2004).
25. G. Panyi, C. Deutsch, Cross talk between activation and slow inactivation gates of *Shaker* potassium channels. *J. Gen. Physiol.* **128**, 547–559 (2006).
26. E. Sadovsky, O. Yifrach, Principles underlying energetic coupling along an allosteric communication trajectory of a voltage-activated K^+ channel. *Proc. Natl. Acad. Sci. U.S.A.* **104**, 19813–19818 (2007).
27. L. G. Cuello, V. Jogini, D. M. Cortes, A. C. Pan, D. G. Gagnon, O. Dalmas, J. F. Cordero-Morales, S. Chakrapani, B. Roux, E. Perozo, Structural basis for the coupling between activation and inactivation gates in K^+ channels. *Nature* **466**, 272–275 (2010).
28. A. C. Pan, L. G. Cuello, E. Perozo, B. Roux, Thermodynamic coupling between activation and inactivation gating in potassium channels revealed by free energy molecular dynamics simulations. *J. Gen. Physiol.* **138**, 571–580 (2011).
29. C. J. Peters, D. Fedida, E. A. Accili, Allosteric coupling of the inner activation gate to the outer pore of a potassium channel. *Sci. Rep.* **3**, 3025 (2013).
30. A. J. Labro, D. M. Cortes, C. Tilegenova, L. G. Cuello, Inverted allosteric coupling between activation and inactivation gates in K^+ channels. *Proc. Natl. Acad. Sci. U.S.A.* **115**, 5426–5431 (2018).
31. L. Coonen, E. Mayeur, N. De Neuter, D. J. Snyders, L. G. Cuello, A. J. Labro, The selectivity filter is involved in the U-type inactivation process of Kv2.1 and Kv3.1 channels. *Biophys. J.* **118**, 2612–2620 (2020).
32. A. Lewis, V. Kurauskas, M. Tonelli, K. Henzler-Wildman, Ion-dependent structure, dynamics, and allosteric coupling in a non-selective cation channel. *Nat. Commun.* **12**, 6225 (2021).
33. C. A. Bassetto, J. L. Carvalho-de-Souza, F. Bezanilla, Molecular basis for functional connectivity between the voltage sensor and the selectivity filter gate in *Shaker* K^+ channels. *eLife* **10**, e63077 (2021).
34. X.-F. Tan, C. Bae, R. Stix, A. I. Fernández-Mariño, K. Huffer, T.-H. Chang, J. Jiang, J. D. Faraldo-Gómez, K. J. Swartz, Structure of the Shaker Kv channel and mechanism of slow C-type inactivation. *Sci. Adv.* **8**, eabm7814 (2022).
35. L. Heginbotham, Z. Lu, T. Abramson, R. MacKinnon, Mutations in the K^+ channel signature sequence. *Biophys. J.* **66**, 1061–1067 (1994).
36. E. Loots, E. Y. Isacoff, Protein rearrangements underlying slow inactivation of the *Shaker* K^+ channel. *J. Gen. Physiol.* **112**, 377–389 (1998).
37. Y. Yang, Y. Yan, F. J. Sigworth, How does the W434F mutation block current in *Shaker* potassium channels? *J. Gen. Physiol.* **109**, 779–789 (1997).
38. J. G. Starkus, L. Kuschel, M. D. Rayner, S. H. Heinemann, Ion conduction through C-type inactivated *Shaker* channels. *J. Gen. Physiol.* **110**, 539–550 (1997).
39. J. G. Starkus, L. Kuschel, M. D. Rayner, S. H. Heinemann, Macroscopic Na^+ currents in the "Nonconducting" *Shaker* potassium channel mutant W434F. *J. Gen. Physiol.* **112**, 85–93 (1998).
40. D. H. Hackos, T. H. Chang, K. J. Swartz, Scanning the intracellular S6 activation gate in the Shaker K^+ channel. *J. Gen. Physiol.* **119**, 521–531 (2002).
41. M. Sukhareva, D. H. Hackos, K. J. Swartz, Constitutive activation of the Shaker Kv channel. *J. Gen. Physiol.* **122**, 541–556 (2003).
42. E. Perozo, R. MacKinnon, F. Bezanilla, E. Stefani, Gating currents from a nonconducting mutant reveal open-closed conformations in *Shaker* K^+ channels. *Neuron* **11**, 353–358 (1993).
43. C. Moscoso, A. Vergara-Jaque, V. Marquez-Miranda, R. V. Sepulveda, I. Valencia, I. Diaz-Franulic, F. Gonzalez-Nilo, D. Naranjo, K^+ conduction and Mg^{2+} blockade in a *Shaker* Kv-channel single point mutant with an unusually high conductance. *Biophys. J.* **103**, 1198–1207 (2012).
44. F. Tombola, M. M. Pathak, E. Y. Isacoff, Voltage-sensing arginines in a potassium channel permeate and occlude cation-selective pores. *Neuron* **45**, 379–388 (2005).
45. F. Tombola, M. M. Pathak, P. Gorostiza, E. Y. Isacoff, The twisted ion-permeation pathway of a resting voltage-sensing domain. *Nature* **445**, 546–549 (2007).
46. J. Thompson, T. Begenisich, External TEA block of *Shaker* K^+ channels is coupled to the movement of K^+ ions within the selectivity filter. *J. Gen. Physiol.* **122**, 239–246 (2003).
47. S. C. Salvage, K. H. Chandrasekharan, K. Jeevaratnam, A. F. Dulhunty, A. J. Thompson, A. P. Jackson, C. L.-H. Huang, Multiple targets for flecainide action: Implications for cardiac arrhythmogenesis. *Br. J. Pharmacol.* **175**, 1260–1278 (2018).
48. D. Choquet, H. Korn, Mechanism of 4-aminopyridine action on voltage-gated potassium channels in lymphocytes. *J. Gen. Physiol.* **99**, 217–240 (1992).
49. G. E. Kirsch, C. C. Shieh, J. A. Drewe, D. F. Vener, A. M. Brown, Segmental exchanges define 4-aminopyridine binding and the inner mouth of K^+ pores. *Neuron* **11**, 503–512 (1993).
50. A. Melishchuk, C. M. Armstrong, Mechanism underlying slow kinetics of the OFF gating current in *Shaker* potassium channel. *Biophys. J.* **80**, 2167–2175 (2001).
51. J. Lopez-Barneo, T. Hoshi, S. H. Heinemann, R. W. Aldrich, Effects of external cations and mutations in the pore region on C-type inactivation of Shaker potassium channels. *Recept Channels* **1**, 61–71 (1993).
52. M. Zhou, R. MacKinnon, A mutant KcsA K^+ channel with altered conduction properties and selectivity filter ion distribution. *J. Mol. Biol.* **338**, 839–846 (2004).
53. C. Tilegenova, D. M. Cortes, N. Jahovic, E. Hardy, P. Hariharan, L. Guan, L. G. Cuello, Structure, function, and ion-binding properties of a K^+ channel stabilized in the 2,4-ion-bound configuration. *Proc. Natl. Acad. Sci. U.S.A.* **116**, 16829–16834 (2019).
54. T. Baukrowitz, G. Yellen, Modulation of K^+ current by frequency and external $[K^+]$: A tale of two inactivation mechanisms. *Neuron* **15**, 951–960 (1995).
55. S. Grissmer, M. Cahalan, TEA prevents inactivation while blocking open K^+ channels in human T lymphocytes. *Biophys. J.* **55**, 203–206 (1989).
56. K. L. Choi, R. W. Aldrich, G. Yellen, Tetraethylammonium blockade distinguishes two inactivation mechanisms in voltage-activated K^+ channels. *Proc. Natl. Acad. Sci. U.S.A.* **88**, 5092–5095 (1991).
57. G. Yellen, D. Sodickson, T. Y. Chen, M. E. Jurman, An engineered cysteine in the external mouth of a K^+ channel allows inactivation to be modulated by metal binding. *Biophys. J.* **66**, 1068–1075 (1994).
58. Y. Zhou, J. H. Morais-Cabral, A. Kaufman, R. MacKinnon, Chemistry of ion coordination and hydration revealed by a K^+ channel-Fab complex at 2.0 Å resolution. *Nature* **414**, 43–48 (2001).
59. T. Hoshi, C. M. Armstrong, C-type inactivation of voltage-gated K^+ channels: Pore constriction or dilation? *J. Gen. Physiol.* **141**, 151–160 (2013).
60. R. Reddi, K. Matulef, E. Riederer, P. Moenne-Loccoz, F. I. Valiyaveetil, Structures of gating intermediates in a K^+ channel. *J. Mol. Biol.* **433**, 167296 (2021).
61. S. Yohannan, Y. Hu, Y. Zhou, Crystallographic study of the tetrabutylammonium block to the KcsA K^+ channel. *J. Mol. Biol.* **366**, 806–814 (2007).
62. Z. Wang, N. C. Wong, Y. Cheng, S. J. Kehl, D. Fedida, Control of voltage-gated K^+ channel permeability to $NMDG^+$ by a residue at the outer pore. *J. Gen. Physiol.* **133**, 361–374 (2009).
63. B. S. Khakh, X. R. Bao, C. Labarca, H. A. Lester, Neuronal P2X transmitter-gated cation channels change their ion selectivity in seconds. *Nat. Neurosci.* **2**, 322–330 (1999).
64. A. Loboda, A. Melishchuk, C. Armstrong, Dilated and defunct K channels in the absence of K^+. *Biophys. J.* **80**, 2704–2714 (2001).
65. C. Tilegenova, S. Vemulapally, D. M. Cortes, L. G. Cuello, An improved method for the cost-effective expression and purification of large quantities of KcsA. *Protein Expr. Purif.* **127**, 53–60 (2016).

66. Z. Otwinowski, W. Minor, Processing of X-ray diffraction data collected in oscillation mode. *Methods Enzymol.* **276**, 307–326 (1997).
67. M. Zhou, J. H. Morais-Cabral, S. Mann, R. MacKinnon, Potassium channel receptor site for the inactivation gate and quaternary amine inhibitors. *Nature* **411**, 657–661 (2001).
68. P. Emsley, K. Cowtan, Coot: Model-building tools for molecular graphics. *Acta Crystallogr. D Biol. Crystallogr.* **60**, 2126–2132 (2004).
69. P. D. Adams, P. V. Afonine, G. Bunkoczi, V. B. Chen, I. W. Davis, N. Echols, J. J. Headd, L. W. Hung, G. J. Kapral, R. W. Grosse-Kunstleve, A. J. McCoy, N. W. Moriarty, R. Oeffner, R. J. Read, D. C. Richardson, J. S. Richardson, T. C. Terwilliger, P. H. Zwart, PHENIX: A comprehensive Python-based system for macromolecular structure solution. *Acta Crystallogr. D Biol. Crystallogr.* **66**, 213–221 (2010).

Acknowledgments: We want to thank S. Russi at the Stanford Synchrotron Radiation Laboratory Beamline (SSRL) 14-1 for assistance at the synchrotron. We want to thank A. Van Tilborg and E. Mayeur for excellent technical support. **Funding:** This work was supported by University of Antwerp DOCPRO Ph.D. funding (to L.C.), Mexican National Council for Science and Technology CONACyT grant 203936 (to E.M.-M.), National Institutes of Health Award R01GM097159 (to L.G.C.), and Ghent University BOF funding (to A.J.L.). **Author contributions**: L.C., E.M.-M., and D.V.V.D.S. performed electrophysiological experiments. L.C., E.M.-M., D.J.S., and A.J.L. analyzed electrophysiological data. D.M.C. and L.G.C. resolved 3D KcsA crystal structure. L.C., E.M.-M., D.J.S., L.G.C., and A.J.L. interpreted results. L.G.C. and A.J.L. conceptualized research. L.C., L.G.C., and A.J.L. wrote the paper. **Competing interests:** The authors declare that they have no competing interests. **Data and materials availability:** All data needed to evaluate the conclusions in the paper are present in the paper and/or the Supplementary Materials. The crystal structure of KcsA-W67F is deposited in the PDB (PDB ID: 7SQW).

Submitted 8 November 2021
Accepted 1 August 2022
Published 16 September 2022
10.1126/sciadv.abn1731